THE ASTROPHYSICAL JOURNAL, 330:38–50, 1988 July 1

INTERACTING BINARY GALAXIES. II. MATCHING MODELS TO OBSERVATIONS

KIRK D. BORNE[1]
Department of Astronomy, University of Michigan, and Space Telescope Science Institute[2]
Received 1985 October 3; accepted 1987 December 23

ABSTRACT

This paper presents an efficient numerical simulation algorithm for the study of interacting elliptical galaxies. Each model galaxy, represented by a collection of gravitating particles, can be (1) endowed with arbitrary degrees of flattening and rotation, (2) oriented in any spatial direction, (3) evolved along any chosen orbital trajectory for an arbitrary length of time, and (4) projected onto the "sky" of a randomly oriented observer. How "observations" of simulated tidal interactions between model galaxies are best matched to the measured properties of real binaries is discussed in detail. Rotation curves, radial variations in velocity dispersion, and surface density maps are all matched to the data in an effort to determine the physical state of an observed pair. Strong support is given to the acquisition of velocity measurements and to their application in any model-matching efforts. That the combined spectroscopic and photometric data for specific binaries can be reproduced by appropriate projections of select numerical simulations of the pairs is demonstrated in the companion papers (Papers III and IV). Each matching simulation constrains the masses of the galaxies, their internal dynamics, the properties of their relative orbit, and the three-dimensional orientation of the pair in space. The uniqueness of such dynamical solutions is discussed in detail in the context of a particular representation of the binary orbits: the specification of their speed and separation at pericenter. It is shown that tidal impulse and duration of pericenter passage are the relevant physical parameters affecting the observed tidal distortions in colliding galaxies. Provided that the images of such systems are supplemented with detailed kinematic data, the study of tidally distorted binary galaxies thus represents a fertile avenue to the direct measurement of galaxy masses.

Subject headings: galaxies: clustering — galaxies: internal motions — galaxies: structure

I. INTRODUCTION

Comparisons between interacting galaxies and reasonably simple numerical models can lead to considerable understanding of the evolution of nonisolated galaxies. In particular, it has been shown that the outcome of ordinary binary encounters is coalescence: the merger of the two galaxies into a single dynamical system (e.g., Borne 1984, hereafter Paper I, and references therein; White 1978, 1979; Farouki and Shapiro 1982; Villumsen 1982, 1983; Negroponte and White 1983; Gerhard 1981; Carlberg 1982). Paper I describes in detail one particular numerical simulation algorithm and some of the results derived from its use. The short merger times (e.g., 10^9 yr) found by other investigators were confirmed in that paper, to within a factor of 2. This time scale implies that many of the galaxies now observed in pairs will soon merge and that a considerable number of pairs have merged in the past (White and Sharp 1977; Toomre 1977). NGC 7252 has been identified as an example of a possible merger remnant (Schweizer 1982; Borne and Richstone 1982, 1988).

In order to test the tidal friction and merger hypotheses, detailed simulations of individual binaries should be attempted. An efficient numerical modeling scheme is required in order to allow a meaningful sampling of the multidimensional parameter space that defines the properties of the galaxies and their relative orbit. Naturally, the validity of these simulations as representations of real binaries is found only in the context of the particular physical model employed. For example, our simulations cannot constrain the amount of dark matter that may be present in a massive halo around any of these galaxies. This is simply because tidal effects like those we see in our systems are observable only when the binary separation is nearly equal to the luminous dimensions of the galaxies. At such separations, the halo makes an insignificant contribution to the tides since most of the dark matter lies outside the luminosity radius of the galaxies. Within the context of our models therefore (i.e., on the scale of the luminous matter), we can derive binary galaxy masses, spatial orientations, orbits, and evolution.

This paper presents the numerical model used in the companion papers (Borne and Hoessel 1988, hereafter Paper III; Borne 1988, hereafter Paper IV) and elsewhere (Borne and Hoessel 1984; Borne, Balcells, and Hoessel 1988, hereafter Paper V) for the dynamical study of particular pairs of interacting galaxies. Particular attention is given to (i) the improvements and modifications made to the model since Paper I and to (ii) the philosophy and method of matching simulations to observations. The multiple three-body algorithm (hereafter, MTBA) of Borne (1979, 1982, and Paper I) finds its most fruitful application in the search-and-fit procedure described in this paper (§ VIII). That is, many simulations can be run efficiently in the effort to find their best match to the observations of a particular binary.

The main attributes of MTBA are presented as follows. Section II consists of both a brief explanation of the algorithm that was used for Paper I and a description of its most significant modifications for use in Papers IV and V. Section III describes the galaxy model and how the perturber (secondary

[1] Visiting Astronomer, Kitt Peak National Observatory, National Optical Astronomy Observatories, operated by the Association of Universities for Research in Astronomy, Inc., under contract with the National Science Foundation.

[2] Operated by the Association of Universities for Research in Astronomy, Inc., for the National Aeronautics and Space Administration.

galaxy) scales with the primary galaxy. The methods by which the model galaxies can be flattened and by which they can receive varying degrees of internal rotation are outlined in §§ IV and V, respectively. Section VI describes the model observations that can be measured on the "sky" of a variably oriented observer. Examples of the various observables (e.g., surface density distributions, rotation curves, and dispersion profiles) are included with the discussion. The free parameters of the problem are identified in § VII, while the procedure by which one begins to search that parameter space for a simulation that matches all of the observations available for a given pair of galaxies is outlined in § VIII. In the final section (§ IX), the uniqueness of the solutions is discussed in the context of a particular two-dimensional cut through the multidimensional model parameter space: the $R_{\rm peri} - V_{\rm peri}$ plane. Also in § IX, the point is made that the success of the method depends on the availability of detailed kinematic measurements across the images of interacting galaxies, particularly at their centers.

II. THE MULTIPLE THREE-BODY ALGORITHM (MTBA)

a) *Highlights of the Method*

Paper I describes the many features of MTBA, the most attractive of which are listed here. (1) The forces of interaction between the test particles and the centers of the two galaxies are explicitly included, which allows for binary orbital evolution and the merger of the pair through energy and angular momentum transfer. (2) The models of the galaxies are subjected to a "proximity relaxation" phase, in which the phase-space distribution function of each galaxy (i.e., the combination of the mass, energy, and angular momentum distributions) is allowed to accommodate the proximity of the companion. (3) MTBA is able to reproduce both the structural properties of postcollision galaxies and to improve on the merger times that have been derived from the much less efficient N-body calculations. (4) For a simulation involving X particles, MTBA requires a factor X less computing than the direct N-body algorithm. This last point is the one that we exploit in Paper IV and in subsequent papers. A large number of simulations can be investigated relatively quickly in order to identify the one set of parameters that best describes the physical state of an observed pair of interacting galaxies.

b) *The Equations of Motion*

The basic equations of motion for MTBA comprise equations (1a)–(1c) of Paper I. In its original form, MTBA permitted investigations of interactions between a primary "galaxy" of particles and a single point-mass perturber. A significant modification to those equations now allows the perturber (hereafter, secondary galaxy) to be represented by a physically realistic distribution of test particles. For the simulations described in Paper IV, the equations of MTBA are

$$m_i \frac{d\boldsymbol{v}_i}{dt} = -m_i M_1 \nabla_i \phi_{i1} - m_i M_2 \nabla_i \phi_{i2} , \tag{1}$$

$$M_2 \frac{d\boldsymbol{v}_2}{dt} = \mu \frac{d\boldsymbol{v}}{dt} = -\mu \nabla_r \Phi , \tag{2}$$

$$M_1 \frac{d\boldsymbol{v}_1}{dt} = -M_2 \frac{d\boldsymbol{v}_2}{dt} . \tag{3}$$

The first and last equations are the same as the corresponding equations in Paper I. Their meanings are likewise identical to those of that paper: each particle responds only to the global, unperturbed fields of M_1 and M_2 (eq. [1]) and global linear momentum conservation is maintained by requiring that $M_1 \boldsymbol{r}_1 + M_2 \boldsymbol{r}_2 = \boldsymbol{0}$ (eq. [3]). Equation (2) differs from the corresponding equation in Paper I in the way that the force on M_2 is calculated: it is derived here from the equivalent one-body representation of the binary system (see next section). This change is necessitated by the addition N_2 test particles to the galaxy M_2, where $N_2 = (M_2/M_1)N_1$. Usually, $N_1 + N_2 \leq 2000$, but as many as 10^4 particles have been included in a few simulations to test the statistical quality of the solutions.

c) *The Equivalent One-Body Problem*

As expressed in equation (2), the solution for the binary orbital motion is reduced to that of an equivalent one-body problem. In this representation, μ is the reduced mass of the binary system, $\boldsymbol{v} = \boldsymbol{v}_2 - \boldsymbol{v}_1$ is the relative velocity vector, $r = |\boldsymbol{r}_2 - \boldsymbol{r}_1|$ is the separation of the galaxy centers, and Φ is the external potential, whose gradient is taken with respect to the binary separation r. Because the internal self-gravity of the two galaxies does not contribute to their mutual acceleration, the binary potential Φ can be represented by

$$\Phi = \sum_i m_i \phi_{i1} + \sum_i m_i \phi_{i2} - \Phi_{\rm self\text{-}gravity} , \tag{4}$$

where the sums are taken over all particles i. This expression is approximately equivalent to

$$\Phi \approx \sum_{i \in M_2} m_i \phi_{i1} + \sum_{i \in M_1} m_i \phi_{i2} , \tag{5}$$

where the first sum is taken only over those particles comprising M_2 and the second sum is taken only over those comprising M_1. In going from equation (4) to equation (5), the self-gravity terms have been assumed to add to zero, as they ought. After a little algebraic manipulation, equation (2) can then be rewritten as

$$M_2 \frac{d\boldsymbol{v}_2}{dt} = \frac{M_2}{M_1 + M_2} \boldsymbol{F}_{21} - \frac{M_1}{M_1 + M_2} \boldsymbol{F}_{12} , \tag{6}$$

where

$$\boldsymbol{F}_{21} = -M_1 \sum_{i \in M_2} m_i \nabla_r \phi_{i1} = -M_1 \sum_{i \in M_2} m_i \nabla_i \phi_{i1} , \tag{7}$$

$$\boldsymbol{F}_{12} = +M_2 \sum_{i \in M_1} m_i \nabla_r \phi_{i2} = -M_2 \sum_{i \in M_1} m_i \nabla_i \phi_{i2} \tag{8}$$

Two distinct representations of the force between M_1 and M_2 are provided by the terms $\boldsymbol{F}_{12}$ and $\boldsymbol{F}_{21}$. $\boldsymbol{F}_{21}$ is the force acting on M_2 as determined by the sum of the external forces (from M_1) acting on the test particles comprising M_2. $\boldsymbol{F}_{12}$ is the force acting on M_1 as determined by the sum of the external forces (from M_2) acting on the particles comprising M_1. The negative of $\boldsymbol{F}_{12}$ is thus the force of reaction back onto M_2. Equation (6) thus represents the total force acting on M_2 as the weighted mean of $\boldsymbol{F}_{21}$ and $-\boldsymbol{F}_{12}$, where the weights are equal to the fractions of the total mass of test particles that contribute to the calculation of each representation of the force. This calculated mean (eq. [6]) very simply allows each particle equal significance in its influence on the dynamical evolution of the binary. Given that $\boldsymbol{F}_{12}$ and $\boldsymbol{F}_{21}$ represent the same force, albeit through two different sets of particles, equation (6) therefore provides a physically reasonable representation of the force of interaction between M_1 and M_2 and is the best possible expression of equation (2) for MTBA. Again, it is derived

directly from the equivalent one-body problem for the reduced mass $\mu = M_1 M_2/(M_1 + M_2)$ of the binary system.

d) The Energy Integral

A simple manipulation of equations (1)–(8) determines the energy integral:

$$\tfrac{1}{2}\mu v^2 + \sum_i m_i(\tfrac{1}{2}v_i^2 + M_1\phi_{i1} + M_2\phi_{i2}) = \text{constant}\,, \quad (9)$$

where v and v_i denote speeds, and $v = |\boldsymbol{v}_2 - \boldsymbol{v}_1|$.

III. THE GALAXY MODEL

The analytic form of the potential ϕ_{i1}, derived in Paper I, is essentially that of an isothermal sphere with an energy cutoff. This provides a physically realistic representation for model galaxies. If M_β denotes a galaxy mass, σ_β it central velocity dispersion, R_β its cutoff radius, and a_β the softening parameter in the expression for its gravitational potential, then the following expressions provide the recipe for constructing galaxies of different scale:

$$G = M_1 = R_1 = 1\,, \quad (10)$$

$$M_2 R_2^{-2} = M_1 R_1^{-2}\,, \quad (11)$$

$$M_2 a_2^{-2} = M_1 a_1^{-2}\,, \quad (12)$$

$$M_2 \sigma_2^{-4} = M_1 \sigma_1^{-4}\,, \quad (13)$$

$$\phi_{i2}(r) = \left(\frac{\sigma_2}{\sigma_1}\right)^2 \phi_{i1}\left(\frac{a_1 r}{a_2}\right), \quad (14)$$

$$\phi_{i2}(r) = \left(\frac{M_2}{M_1}\right)\left(\frac{R_1}{R_2}\right)\phi_{i1}\left(\frac{R_1 r}{R_2}\right). \quad (15)$$

The expression for ϕ_{i1} can be found in equation (15) of Paper I. As in that paper, a value $a_1 = 0.05$ is used in the calculation of the potential. Therefore, a value for M_2 is sufficient to define all of the properties of the secondary galaxy with respect to the primary galaxy M_1.

Equation (10) defines the dimensionless units of the model. Equations (11) and (12) are somewhat arbitrary, although they imply a unique surface brightness for all galaxies (provided M/L is the same for all). Equation (13) follows from the constant M/L assumption and the observed Faber-Jackson relation (1976; Terlevich *et al.* 1981). Equations (14) and (15) are based on the assumption that the initial galaxy models are homologous: derivable from a single scale-free model. Davies *et al.* (1983) have shown that this is not at all unreasonable for a major fraction of elliptical galaxies. They present relationships derived from their data that are consistent with equations (11) and (13). Scale-free models may even work for spiral galaxies; Burstein and Rubin (1985) have demonstrated the uniformity in the shapes of the mass distribution functions for an otherwise nonuniform sample of spirals. It appears then that our use of scale-free models is quite reasonable.

IV. FLATTENING OF THE MODEL GALAXIES

Unlike the model galaxies of Paper I, either M_1 or M_2 (or both) can be flattened by an arbitrary, though uniform, factor along an arbitrary minor-axis direction. Each galaxy is transformed independent of the other. For simplicity, no corresponding change in the analytic form of the potential is made for any of the flattened configurations, which is not unreasonable given the weak dependence of the potential on the flattening of the spatial density law. If ϵ is the usual flattening parameter (i.e., ellipticity) for a galaxy and if $\boldsymbol{u}_\epsilon$ is the unit vector along the minor axis, then the position and velocity vectors $\boldsymbol{s}_i$ of each particle in the initially spherical configuration for the given galaxy are transformed according to

$$\boldsymbol{s}_i^{\text{new}} = \boldsymbol{s}_i^{\text{old}} - \epsilon(\boldsymbol{u}_\epsilon \cdot \boldsymbol{s}_i^{\text{old}})\boldsymbol{u}_\epsilon\,. \quad (16)$$

For example, an E7 galaxy is obtained from the initially spherical particle distribution by using the coordinate transformation in equation (16) with a value $\epsilon = 0.7$. That transformation is simply a multiplication by $(1 - \epsilon)$ of the position and velocity coordinates along the prescribed axis in the initially spherical model galaxy. Positions and velocities for all of the test particles within the given galaxy are so transformed.

The flattening transformation that is represented by equation (16) results in a nonequilibrium initial state. This configuration is allowed to relax in an isolated-galaxy "mixing phase" prior to the binary "proximity relaxation" phase, which itself precedes the full binary "interaction phase" (see Paper I for a full discussion of these various phases of the simulations). As a consequence of mixing and relaxation, the flattened system of particles moves to an equilibrium configuration whose ellipticity differs slightly from the value of ϵ that was used to construct the initial model galaxy. Our flattening algorithm essentially introduces a nonclassical integral of motion to the system of particles. By artificially suppressing the component of the velocity dispersion parallel to the minor axis, this confining integral limits the extent to which particles can travel from the galaxy's initial plane of symmetry. Even though the initial state (as transformed by eq. [16]) is not one of stable equilibrium, the mixed preencounter configuration is in equilibrium and satisfies the Jean's theorem requirement for the phase-space distribution function to depend solely on the isolating integrals of motion.

V. ROTATION IN THE MODEL GALAXIES

If a rotating model galaxy is desired, then one of three modes of rotation can be selected. The three are described below. Of these, the last one to be presented (§ V*c*) seems to work the best in simulating the galaxies observed for Papers III and IV. As is the case when flattening is introduced (see discussion at the end of the previous section), the initial rotation conditions place the galaxy in a nonequilibrium state. What is then necessary is that both a "mixing" and a "proximity relation" phase be applied to the models prior to the binary encounter, forcing the stellar phase-space distribution function into a stable configuration that is consistent with the presence of a massive companion galaxy. Self-consistent flattened and rotating models (e.g., those of Wilson 1975) are not used here since it is abundantly clear that elliptical galaxies are not supported (or flattened) by rotation (Illingworth 1981, and references therein), as those models assume. Clearly, a record of the initial formation conditions remains in elliptical galaxies where the degree of flattening and rotation are only weakly correlated, if at all. Accordingly, we take the simple approach here of avoiding such complicated models, even though they do provide for a self-consistent description of flattened galaxies. We merely impose some useful boundary conditions on the initial particle distribution (§ IV) and on the initial rotation properties (this section), for one (or both) of the model galaxies, and then allow the systems to relax before proceeding with the binary encounter simulation.

When both nonzero ellipticity and rotation are desired in a given model galaxy, the flattening transformation (eq. [16]) is applied first, followed by the addition of rotation. Particle velocity components that are parallel to the galaxy minor axis are thereby constrained to be consistent with the spatial flattening (see § IV). The rotation component of the particle velocities can take one of three forms, as will now be described.

a) Rigid Rotation

Paper I allowed a rigid rotation to be superposed on the random motions of the test particles comprising M_1. The angular rate and direction of the rotation were restricted to that of the binary orbit. No such restrictions exist in the version of MTBA described in this paper, where an arbitrary rigid rotation rate about any axis in either or both of the model galaxies is allowed.

b) Circular Rotation

In the circular rotation mode, each particle is assigned the circular velocity at its initial radius. This motion is around a randomly selected rotation axis that is unique to that particle. The rotation axes for all of the particles are constrained to point into the same half-space. That is, if $\boldsymbol{u}_\Omega$ denotes a unit vector along the net rotation axis for the entire galaxy and if $\boldsymbol{\Omega}_i = \boldsymbol{r}_i \times \boldsymbol{v}_i$ defines the rotation axis for a particular particle orbit, then

$$\boldsymbol{u}_\Omega \cdot \boldsymbol{\Omega}_i > 0 \qquad (17)$$

is required of that particle, and so on for each additional particle in that galaxy. This yields a nonzero net galactic rotation about an axis parallel to $\boldsymbol{u}_\Omega$. Note that the particles are not constrained to follow a circular trajectory, which is strictly impossible for our binary gravitational potential. Particles are simply given a speed that is consistent with circular motion at their initial radial distance from the center of the galaxy.

c) Net Rotation by Reflection of Velocities

A reflection algorithm can also be used to generate rotation in the model galaxies. In this case, the initially assigned random motion of each particle is left intact except that the parity of the initial velocity vector is set by constraining equation (17) to be satisfied for each and every particle in the galaxy. Even though this algorithm in no way changes the energy dependence $f(E)$ of the initial particle phase-space distribution function, the model is no longer an isotropic one, as was originally assumed in constructing the galaxy. Note that the entire form of the phase-space distribution function changes whenever the rigid rotation or circular rotation mode is selected. Even so, any complications imposed on the physical model by rotating the galaxies have been ignored here. (An independent study should be undertaken to assess the significance and relevance of such modifications to the phase-space distribution function.) Since the reflection formula represents, among the methods introduced in this section, the one technique that is most faithful to the original physical model, it is both expected and found to be true that galaxies set in rotation by this algorithm will most resemble real elliptical galaxies (see Paper IV).

d) Choosing a Mode of Rotation

A rotation mode is selected for each galaxy independently of the other. The rotation and minor axes of a galaxy are not forced to be parallel, although the two axes normally do coincide. Rotation may be either retrograde or prograde with respect to the relative trajectory of the two galaxies. In fact, the rotation may be at any angle (parallel, antiparallel, orthogonal, or oblique) to the binary orbital revolution. Furthermore, one can specify what fraction of the total number of particles in a given galaxy will participate in the rotation; the remainder of the particles will retain the random velocity distribution that is imposed on them by the initial model. Obviously, if one chooses, the "no rotation" option can be selected for either of the galaxies.

Given the many rotation options from which to choose, a dynamical configuration for the particles can usually be found that matches the observed rotation curve in the inner regions of a given galaxy. It is at those small radii that the gravitational tides have least affected the initial rotation properties of the galaxy, and that is where we can hope to discern clearly the internal dynamical properties of the individual galaxies in an interacting pair. The external dynamical properties of the pair as a whole tangle with the internal galaxy dynamics when studying the observed rotation velocities in the disturbed outer regions of binary galaxies. Model rotation velocities at these large radii generally match the observed data best following a period of tidal interaction between the model galaxies.

VI. MODEL OBSERVATIONS

In order to facilitate the matching of numerical models to the observational data, MTBA has been set up to run interactively with extensive graphics display capabilities. An interactive graphics package is used to plot projected mass and velocity distributions: individual particle distributions, "surface brightness" contour maps, rotation curves, velocity dispersion profiles, integrated line-of-sight velocity distributions, and two-dimensional velocity maps. Such "observations" can be examined from an arbitrary viewing angle at any time during the numerical simulation. Examples of some of these are presented below.

a) Projected Mass Distributions

From any direction in space, an "observer" may plot the projected positions of the test particles or draw a surface density contour map. For the surface density maps, contours are drawn at intervals of 1 mag per square pixel. Pixels are square and 0.05 units wide (units defined by eq. [10]), where $a_1 = 0.05$ is the softening radius for galaxy M_1. Several examples of the projected particle configuration from a particular integration are shown in Figure 1. The particle distribution shown in the upper left box corresponds with the contour map displayed in the upper left box of Figure 3. Each of the boxes in these figures is 6.0 distance units on a side, where the effective radius of the initial galaxy model was 0.20 units (eq. [20] of Paper I). For the integration displayed in Figure 1, $N_1 = N_2 = 1000$, and the galaxies were placed on an initially circular orbit of unit radius.

At the time of observation in Figure 1, the galaxies have completed one-half of their first orbit. The observer for the distribution in the upper left box of Figure 1 is viewing the interaction pole-on. From this point of observation, down the orbital angular momentum axis, the galaxies are revolving counterclockwise. Note that the tidal disturbances in each galaxy are *following*; there is no significant *leading* tidal component. That is, the majority of the "excited" stars occupy the first and third quadrants of Figure 1, with few exceptions. Those particles now seen in the first quadrant (i.e., following

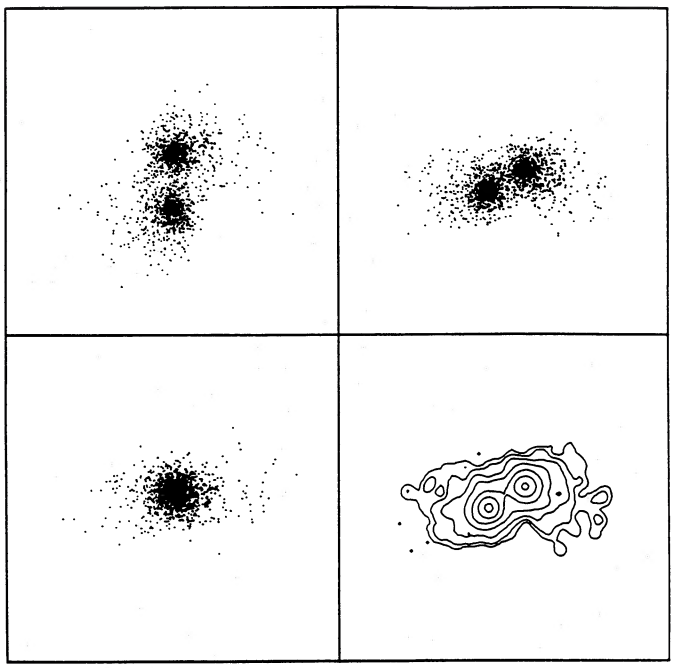

FIG. 1.—Views of a simulation in which $N_1 = N_2 = 1000$. The binary separation is 1.0 distance units, where each box is 6 units on a side (units defined by eq. [10]). Upper left box shows a top view of the particle distribution; the corresponding contour map appears in the upper left box of Fig. 3. Particle distribution in the bottom left box is that seen from the orbital plane along the line connecting the galaxy centers. An oblique view of the particle distribution and the corresponding surface density contour map are displayed in the upper right and lower right boxes, respectively.

the upper galaxy) did, in fact, originate in that galaxy, and those following the lower galaxy originated in it. An observer in the orbital plane along the line connecting the galaxy centers would see the view reproduced in the lower left box of Figure 1. Note that the distribution of disturbed particles is distended parallel to the orbital plane, which is the usual tidal effect wherein the perturbing forces tend to constrain motions in the vertical direction while enhancing motions horizontally. An oblique view of the same particle configuration is portrayed in the upper right box of Figure 1: the observer in this case is 60° away from the pole (i.e., 30° above the orbital plane) and is at a phase 45° ahead of the lower galaxy seen in the upper left box. A surface density contour map for this particle distribution is shown in the box below it. This map looks very similar to the surface brightness map of the galaxy K564 shown in Figure 7 of Paper III. If imaging data alone were available for a pair of galaxies like K564, then one would be satisfied with the excellent match demonstrated by this simulation. Unfortunately, when the rotation curves of the model galaxies are calculated, the so-called match is seen to be a failure (see below). This was found to be a very general occurrence when running simulations: matches to the imaging data were easy to obtain, and they were plentiful. Fortunately, for the purposes of finding unique solutions and galaxy masses, the abundant supply of nonunique imaging solutions was effectively pared down to a very restricted sample of dynamical solutions when velocity data were also used to constrain the set of viable simulations.

b) Velocity Curves

From any direction in space, an "observer" may measure various forms of the velocity distribution (see opening remarks to this section). Of most usefulness in the study of interacting ellipticals are the radial variations of mean line-of-sight velocity and velocity dispersion. The free parameters are the slit location, width, and position angle. Typically, the slit is placed along the line connecting the galaxy centers, and the slit is centered on the system center of mass. For the models described here and in Paper IV, the slit length is fixed at 4.0 distance units. Because of the small numbers of particles involved in the simulations, velocity curves are typically calculated with slit widths ranging from 0.1 to 0.4 distance units (one-half to two galactic effective radii). This would be a ridiculously large slit to use on a real galaxy (where one has to worry about seeing and instrumental resolution), but such widths are necessary in these models to minimize the small-numbers fluctuations in the simulated velocity curves. Each particle within the slit boundaries is assigned to a particular radial bin (i.e., a column of pixels) which runs orthogonal to the long axis of the slit. The assignment is made independent of how far the given particle is above or below the central line defining the slit position.

Velocity curves for the model galaxies depicted in Figure 1 are presented in Figure 2. These are for the oblique-angle observer whose view of the system is shown on the right side of Figure 1. The rotation curve is plotted in the lower panel, with the corresponding velocity dispersion profile in the upper panel. In these figures, as in all of the simulated velocity profiles shown in Paper IV, the units are those defined by equation (10); a convenient transformation to physical units was given in equation (6) of Paper I. The two sets of curves in the lower panel of Figure 2 correspond to $v_r + \alpha_r$ and $v_r - \alpha_r$, where $\alpha_r^2 = \sigma_r^2/N_r$. N_r denotes the total number of particles in a radial bin contributing to a particular point on the velocity profile and v_r and σ_r denote the mean line-of-sight velocity and the line-of-sight velocity dispersion, respectively, at that point. Similarly, the two curves drawn in the upper panel of Figure 2 correspond to $\sigma_r + \beta_r$ and $\sigma_r - \beta_r$, where $\beta_r^2 = \sigma_r^2/2N_r$. The

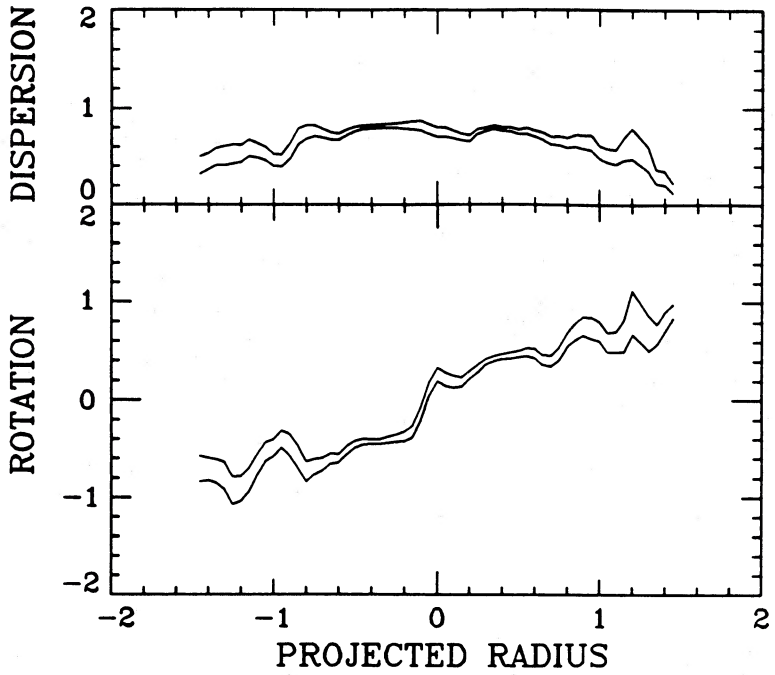

FIG. 2.—Long-slit velocity profiles for the "galaxies" in Fig. 1 as seen by the observer with the oblique view (right side of Fig. 1). The slit passes through the centers of the two galaxies. Radial variations in mean line-of-sight velocity are plotted in the lower panel. Radial variations in line-of-sight velocity dispersion are plotted in the upper panel. Double solid lines are plus and minus one standard deviation from the calculated velocities. Units are defined by eq. (10).

parameters α_r and β_r are the standard errors of the mean velocity and of the velocity dispersion at a given slit position, respectively.

At the time of observation in Figure 2, the projected separation of the galaxies is 0.8 units, so that the centers of the galaxies in that figure are at projected radii -0.4 and $+0.4$, which is where one sees the minimum deviation in the two error curves. Note that the projected relative velocity of the pair is ~ 0.9 velocity units, roughly equal to the central projected velocity dispersions. The near correspondence of these numbers argues against this being a very good viewing angle for the pair of galaxies K564 in Paper III whose relative velocity of 26 km s^{-1} is a tiny fraction of the galaxies' velocity dispersions (~ 180 km s^{-1}).

Figure 2 also demonstrates the effect of tidal torques on the model galaxies. There is a net rotation among all of the particles, exclusive of their relative orbital motion. In addition, the velocity dispersion profiles are a fairly flat function of radius. Given that the initial model galaxies actually had dispersion profiles that decreased significantly with radius, the observed flatness is indicative of tidal heating of the particles in the outer parts of these galaxies.

VII. THE FREE PARAMETERS

The fundamental belief behind our model-fitting procedure is that the abundance of information carried in the data ought to place strong constraints on the range of acceptable values for a fairly large number of model parameters. Given a scale-free galaxy model for which an analytic form for the gravitational potential and a specific energy dependence in the particle phase-space distribution function are prescribed, each simulation will depend on three sets of parameters, to be described below. These are (1) the binary orbital parameters, (2) the internal rotation and flattening parameters, and (3) the angles that define the spatial orientations of all these with respect to the observer. The match between theory and observation ought not and does not depend on which particular statistical realization of the chosen distribution function is selected.

a) Observer Viewing Angle

The location of the observer with respect to the many spatial parameters of the galaxy pair is usually well determined. To be sure, a simulation is not pursued to any length if a good viewing angle for the observer cannot be isolated. A good viewing angle is one that not only provides the correct projected separation and relative velocity, but it also reveals the proper photometric distortions and the correct shapes for the rotation curves. Since the observed relative velocity of the binary is a fixed scale-free fraction of the central velocity dispersions, the range of possible viewing angles is strongly restricted. The choice of observer orientation is even further restricted by the requirement that the projected appearance of the simulated galaxies be compatible with the observed binary.

b) Binary Orbital Parameters

Like the observer viewing angle, the binary orbital parameters are nearly always well constrained. These are R, M_2, and the relative velocity vector, where R is the true binary separation and M_2 is the mass ratio ($M_1 = 1$). Another representation of the orbit parameters would list R, M_2, a, and e, where a is the binary semimajor axis and e is the orbital eccentricity. Similarly, one could specify R, M_2, $R_{\rm peri}$, and $V_{\rm peri}$, where the last two quantities are the pericenter separation and pericenter speed, respectively. Each of these parameters is tightly constrained by the data because of the strong mass and distance dependences of the tidal interaction terms and because the velocity scale is set by the internal velocity dispersion measurements. More will be said in § VIII on how these constraints work to bring about a reasonable match to the data.

Because the observer orientation and the binary orbital parameters are usually well determined, it is a simple matter to calculate total masses and true separations for the galaxies in the observed binary sample. From these numbers, estimates of binary orbital periods can be made, as can estimates of the expected merger timescale for the systems. The calculation of the latter assumes that the relevant timescales determined from interacting galaxy simulations are physically sound (see Paper I). This latter assumption is strongly supported by the demonstration in Paper IV (and subsequent papers) that the gravitational interaction hypothesis is sufficient to account for all of the observations of these interacting binaries.

c) *Internal Galaxy Parameters*

The internal parameters that can be selected for each model galaxy are the flattening, the angles defining the direction of the minor axis, the mode of rotation (see § V), the direction of the rotation axis, and the fraction of particles participating in the rotation. Something will be said about each of these parameters below. Unfortunately, their values are often only weakly constrained by the observations. If the galaxy has nonzero ellipticity and shows rotation along the slit, then something more can be said about the dynamical configuration for that galaxy than for a galaxy with very little rotation or with nearly zero ellipticity around its center. Typically, the internal parameters for each galaxy are constrained not only by the appearance of the galaxy, but also by the ability or inability of a given model configuration to develop, over the course of a simulation, bulges and tails that are similar to those that are seen in the picture data or to develop rotational properties that are similar to those seen in the long-slit spectroscopic data. Only certain models will develop into a configuration that matches all these data.

i) *Flattening*

If the galaxy is intrinsically flat, but the direction of the observer is nearly along the minor axis, then it is difficult to derive the degree of flattening from the procedures described in this paper. In fact, the intrinsic flattening is hard to determine from any angle of observation. A lower limit on its value can be set from the observed ellipticity. Of course, this is neither an original suggestion nor a particularly enlightening one. The true spatial direction of the minor axis for a galaxy with moderate flattening is somewhat better constrained by the simulations than the degree of flattening. This is because the behavior and development of the isophotal twists and tails over the course of the numerical simulation depend on the true direction of the minor axis relative to the line of sight.

ii) *Rotation*

The mode of rotation chosen for most of the galaxy models tabulated in Paper IV is that generated by the reflection algorithm (§ V*c*). Of the three modes of rotation described in § V, this is the only one that preserves the original, physically reasonable, energy dependence of the phase-space distribution function. The dynamical development of tidal distortions in a galaxy with the circular rotation mode is incompatible with what is now seen in the two galaxies described in Papers III and IV (i.e., Karachentsev 1972 Nos. 99 and 564). Likewise, when the rigid rotation mode is employed, the initial galaxy model is not in a steady state configuration, so that the rotational velocity data late in a simulation do not fit the observations nearly so well as they do early in the simulation.

Both the direction of the rotation axis and the fraction of particles actually participating in the rotation for a particular simulation will determine the shape, gradient, and peak-to-peak velocity range in the observed rotation curve. It is therefore possible to place some restrictions on the internal dynamical parameters of the observed galaxies, provided that the three-dimensional velocity distribution in the model is a sensible representation of that in the real galaxy.

iii) *Velocity Dispersions*

The detailed radial variations in the line-of-sight stellar velocity dispersion (e.g., Figs. 4 and 8 of Paper III) are not used extensively in the attempt to match models to the data, except that the central dispersions are used to calibrate the velocity scale for the binary. Once calibrated, the projected relative velocity of the binary constrains the possible projection angles of the total relative velocity vector. The shapes of the velocity dispersion profiles depend on the velocity distribution function within the pre-collision galaxy, about which very little is known. The distribution function used in our models is a physically reasonable one, but it is not necessarily the correct one.

VIII. THE MATCH GAME

It is useful to describe the method by which simulations of interacting model galaxies are matched to a given set of observations (e.g., see Paper IV). A few physical arguments are presented below in order to demonstrate how a reasonable matching model for a specific binary can be isolated among the plethora of possibilities available in our multidimensional parameter space.

a) *The Tidal Strength*

If one attempts to simulate an observed pair of interacting galaxies with a model whose binary separation is too large, then the resulting tidal field in the simulation will be too weak to bring about the degree of distortion that is seen in the light distribution. Yet if one suggests a separation that is too small, then the tidal distortions in the simulation may greatly exceed those that are observed. In the latter case there also will be a crowding of the two galaxies and of their isophotes to the point that the picture data just cannot be matched. A reasonable guess can therefore be made for the value of the true separation, with the exception of those cases where the orbital eccentricity is large (i.e., where the time derivative of the tidal field is not small over the course of the integration). The effects of varying eccentricity are discussed below. To begin the process of isolating a good simulation for a particular binary, one examines the isophotal distortions over the course of the integration. In particular, one views the simulation only from viewing angles that satisfy the requirement that the projected separation of the galaxies (in terms of their half-mass radii) matches that which is observed. If the distortions observed at such viewing angles are too large compared to the distortions observed in the real data, then one would conclude that the true separation of the pair must significantly exceed its observed projected separation on the sky in order for the tidal distortions not to be so strong. If, on the other hand, the distortions observed in the simulation are too small relative to those in the real data, then the true separation of the pair must be less than that in the simulation, with the observed projected separation consequently being a larger fraction of the true separation in space. Following this line of reasoning, it is possible to place tight restrictions (better than 10%) on the range

of acceptable binary separations and, consequently, on the full three-dimensional orientation of the pair.

The interplay between projection and tidal effects is demonstrated in Figure 3 where surface density maps from three different simulations are portrayed: each of these models had unit mass ratio, with the galaxies on initially circular orbits. The initial radii of those orbits were, from left to right: 1.0, 1.2, and 1.4 model units (or five, six, and seven effective radii, respectively). Top views of these interactions are shown in the top row after each pair has completed one half of their first orbit. The contour map shown in the upper left box corresponds with the particle distribution displayed in the upper left box of Figure 1. Note the decreasing tidal effect in these pairs as orbit size increases. Also note that all of the pairs are moving counterclockwise in this figure, so that those tidal bulges that do appear are generally *following* each galaxy. Even though the tidal distortions of the galaxies in the central simulation are weak, that they are *following* is not in doubt. On the other hand, it is not clear that any tidal effects are evident in the rightmost simulation. The bottom row of maps are oblique views of the same models at the same times, but at the particular observer viewing angles for which the projected (i.e., "observed") separation in all three cases is 0.8 model units (four effective radii). The effects of the differing tidal strengths (i.e., orbit sizes) are still visible in the shapes of the contours in these oblique views: from strong distortions in the leftmost simulation, to weak boxlike distortions in the central model, to almost no asymmetry in the galaxies on the right. It should be possible to compare the distortions observed in a real interacting binary with sets of maps like these, from which one could place significant restrictions on its orbit size and on the orbital inclination. Applying velocity constraints to the models would further limit the allowable range of orbital parameters and galaxy masses.

Hoessel, Borne, and Schneider (1985) noted the boxiness of the surface brightness isophotes in the multiple-nucleus galaxy at the center of A1185 and argued that such is an indicator of gravitational interaction among the galaxies in that system. The boxiness seen in the isophotes of the bottom middle map of Figure 3 supports their conclusion.

b) Time-dependent Tides

The orbital eccentricity for an observed pair cannot be determined very well quantitatively through simulation. However, a reasonable qualitative estimate can be made. If the relative trajectory of a simulated pair is highly eccentric, then the relative velocity of the galaxies will be very large at pericenter. In this case, it may not be possible both to match the observed velocity difference and to have a good match to the other observables: prior to closest approach, the tidal forces usually have not affected either galaxy enough to match the observations. In contrast, after closest approach, there may be far too much tidal damage in the system. These arguments do not apply to those cases where the orbital eccentricity is moderate to small. One then must judge from the appearance of a particular simulation if the distortions, the magnitude of the projected relative velocity, and the line-of-sight velocity field of the real galaxies are all consistent with the relative orbit of the pair lying on the chosen trajectory. Clearly, these represent a nontrivial and somewhat subjective set of comparisons that must be made. The task is further complicated in that most of the distortions of interest are being mapped by the very few particles located in the outer parts of the simulated galaxies. This last point is not really as severe a problem as it appears

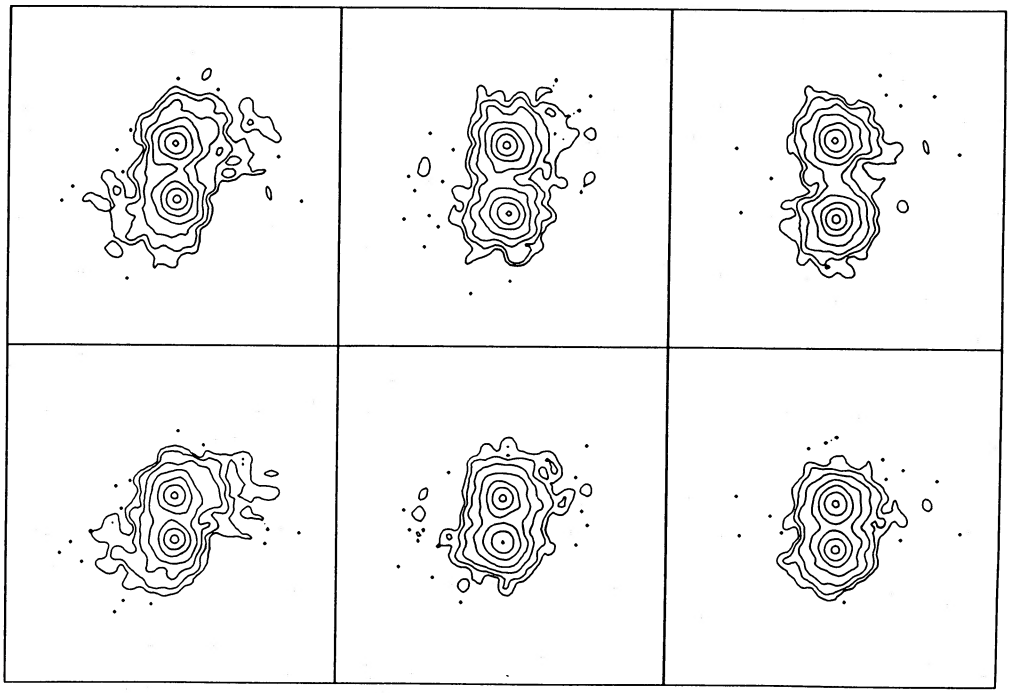

FIG. 3.—Surface density contour maps for the particle distributions from three simulations. Upper boxes are pole-on views of the three models whose binary orbit increases in size going from left to right. Lower boxes are inclined views of the galaxies shown immediately above them; the inclinations are such that the projected separations of the binaries across the bottom row of maps are all equal. Particle distribution corresponding to the map in the upper left box is presented in the upper left box of Fig. 1. Each box measures 6 units on a side. Contours are drawn at intervals of 1 mag per square pixel. A pixel is 0.05 units square. Units are defined by eq. (10).

since there is in reality no particular upper limit to the number of test particles that can be used with a linear code like MTBA. In some cases, a model that matched well to the observations was rerun with many more test particles, thereby confirming the validity of the simulation as a good match to the data.

Simulations in which the binary is in a circular orbit are usually among the first that we investigate. If the "photometric" distortions in one of these simulations are too small, then a smaller circular orbit is investigated. If the distortions are too large, a larger circular orbit is tested. If the actual shapes and twisting of the simulated isophotes differ from those seen in the data, then this is usually an indication that we need something more. Either some degree of eccentricity is needed in the binary trajectory or some flattening and rotation are needed in the model galaxies. Typically, the former possibility is examined first, and is usually sufficient to reproduce the observed distortions. The incentive to add rotation and flattening to the model galaxies primarily derives from attempts to match the properties observed in the unperturbed inner regions of the real galaxies.

c) *Projection Angles and Total Masses*

Where is all this leading us? We are hoping to constrain the three-dimensional orientation of a given pair of interacting galaxies and, therefore, to determine the mass of the pair. This requires us to constrain the projection factors for the relative velocity and separation vectors. Fortunately, these requirements are easily met. The projection factor for the separation vector is constrained by the procedures described in the preceding paragraphs. The projection factor for the relative velocity vector is found by applying a different, but equally successful, set of constraints. Although the radial variations in velocity dispersion are not crucial to the problem (see § VII*c*[iii]), the central dispersions are very important. There is a cone of viewing angles along which the line-of-sight component of the binary relative velocity is a fixed fraction of the central dispersions. Similarly, there is another cone of viewing angles for which the projected binary separation is a fixed multiple of the effective radii of the galaxies. Except for the case of a purely linear binary trajectory, these two cones intersect at most along two lines of sight. (Note that the tidal distortions in a linear encounter of two weakly rotating galaxies are symmetric about the line, and consequently, one can dismiss this type of orbit immediately for the asymmetric pairs of interacting binaries that are the subject of this investigation.) Except for a limited period of time during the simulations, the two cones do not intersect at all. For example, at large separations (where the binary spends most of its life), the total relative velocity may be so low that either a very narrow cone of viewing angles or else no viewing angle will give the desired value of the projected velocity, and, in addition, only on another very narrow cone of viewing angles will the projected separation be a small enough fraction of the total separation to match the observations. For the limited time that the two cones do intersect, usually only one of the two lines of intersection will correspond to a line of sight for which the distortions in the image of the disturbed galaxy pair have the right parity. More often, when the cones intersect, the distortions will not have the correct shape and magnitude, and the search for a good matching model must continue with another set of orbital parameters.

An example of how the projection angles are determined in actual practice follows. One first determines for a particular simulation what orbital inclinations and phases give the correct projected binary separation $S_{\rm proj}$ (in units of $R_{\rm eff}$, the effective radius for the larger galaxy). The projected relative velocity $v_{\rm rel}$ of the model is then calculated for one particular set of observer viewing angles. If the velocity scale is set too high by reason of our line of sight to the simulated pair being parallel to too much of the total relative velocity vector, then the model value for $v_{\rm rel}/\sigma_1$ will be larger than that observed (where σ_1 is the central dispersion of the larger galaxy) and one must decrease the line-of-sight component of the relative velocity. If the velocity scale is set too low by reason of our line of sight being parallel to too little of the relative velocity vector of the simulation, then $v_{\rm rel}/\sigma_1$ will be too low and one must increase the line-of-sight velocity component. Following these guidelines, one can isolate the projection angles, if any are possible, that give the correct values of both $v_{\rm rel}/\sigma_1$ and $S_{\rm proj}/R_{\rm eff}$. Typically, this procedure allows the velocity projection factor (that is, the ratio of total relative velocity to observed line-of-sight relative velocity) to be constrained to within 10% of its actual value.

Because the projections of the relative velocity vector and of the separation vector for observed interacting binaries are both determined to better than 10%, total masses ($\propto S_{\rm proj} v_{\rm rel}^2$) can easily be estimated to within 30%. Since it is the velocity dispersion data that are really responsible for setting the mass scale, significant uncertainties in the relative velocity measured for a given pair (e.g., K564 in Paper III) will not affect the mass calculated for the system as much as much as it will affect the determination of the three-dimensional orientation of the pair relative to the observer. But if the relative velocity is really so small that it nearly equals the error in its measurement, then we know that we must be observing the pair almost pole-on. Hence, the orientation is determined trivially.

IX. UNIQUENESS OF THE SOLUTIONS

For any binary orbit, the dynamical configuration is determined by the mass ratio and two orbital parameters (see § VII*b*), where the latter may be eccentricity and semimajor axis, or they may be the speed and separation at closest approach (pericenter). To specify fully the spatial configuration of an observed pair, additional parameters are required: the current physical separation of the pair (or, equivalently, the orbital phase in the specified orbit) and the spatial orientation of that orbit. These dynamical and spatial variables are the free parameters that one must vary in the search for a simulation that best fits all of the observations. It becomes clear that the spatial orientation of an otherwise acceptable orbit is uniquely determined when one realizes that the projection of the separation vector onto the sky and the projection of the relative velocity vector onto the line of sight will match their observed values typically for either zero or two viewing angles (see § VIII*c*). One must vary the orbital parameters until the number of such viewing angles differs from zero. Then, from the two possible viewing angles, one can trivially select the correct view since the parity of the distortions in the model image will match those observed for only one of the two views. Orbital phase (and, hence, the three-dimensional separation) is likewise well determined for a given orbit when one considers the discussion of § VIII*b*: the time development of the tidal distortions is such that a particular set of observations automatically selects the time of observation for a particular orbit (i.e., for a particular time dependence of the tidal potential).

Having guaranteed the uniqueness of the spatial parameters

for a given orbit, one is then forced to constrain the dynamical parameters of the orbit. Selecting trial solutions by a random trial-and-error search of the corresponding parameter space does not guarantee the uniqueness of a working simulation; although one gains an intuitive belief that the solution is unique, more than intuition is required to demonstrate conclusively that this is so. A particular tool that has proved very helpful in the search for a valid orbital solution and in demonstrating its uniqueness is represented by the $R_{\rm peri} - V_{\rm peri}$ diagram of Figure 4. For a given mass ratio, every possible orbit is completely specified by a point in this plane. The particular coordinate values in Figure 4 correspond to a mass ratio of $M_2/M_1 = 1/3$. To help demonstrate the utility of this diagram, several lines and curves have been drawn through it; each of these will now be described. For a given pericenter separation, there is a minimum pericenter speed that corresponds to the circular orbit at that radius; a slower speed would allow the pair to fall closer than the pericenter separation, an obvious contradiction. The hatch region occupying the entire bottom-left region of the figure is this forbidden domain. Circular orbits occur on the right boundary of that region. The curve delineated by a string of asterisks represents parabolic, zero-energy, encounters for which $V_{\rm peri}{}^2 \propto R_{\rm peri}{}^{-1}$. All points to the right of that curve represent unbound hyperbolic trajectories, while points between that curve and the hatch region represent bound elliptical trajectories. A simple separation of binary interactions into weak and strong collisions would distinguish between (i) bound, slow encounters where the tidal perturbations are strong and of long duration, and (ii) unbound, fast encounters where the tides are weak and short-lived. A more quantitative description demands a measure of the tidal impulse:

$$W_{\rm tidal} \approx F_{\rm tidal}\,\Delta t \propto \frac{1}{R_{\rm peri}{}^2} \cdot \frac{R_{\rm peri}}{V_{\rm peri}} = \frac{1}{R_{\rm peri}\,V_{\rm peri}} . \qquad (18)$$

The first proportionality assumes that the tidal force $F_{\rm tidal}$ varies as x/d^3, where x is the radius at which most of the tidal effects occur and $d = R_{\rm peri}$ is the separation of the galaxies at the moment when the tides are strongest. For collisions in which the galaxies interpenetrate, $x \approx R_{\rm peri}$. From equation (18), we see that the tidal impulse per unit mass is inversely proportional to the orbital angular momentum per unit mass. Curves of constant $W_{\rm tidal}$ therefore correspond to curves of constant specific angular momentum where $R_{\rm peri} \propto 1/V_{\rm peri}$. Three such hyperbolae are shown in Figure 4 for which $(R_{\rm peri}\,V_{\rm peri})^{-1} = 3/4$, 1, and 4/3. As tidal impulse weakens (i.e., as the product of the tidal force and its duration decreases), the curves of constant impulse progress toward the upper right in the $R_{\rm peri} - V_{\rm peri}$ diagram. Our initial qualitative separation of collisions into strong and weak on the basis of the boundness of the trajectory is thus slightly modified by this quantitative estimate of the tidal impulse: a very strong, yet unbound, encounter is possible when the pericenter separation is very small, and conversely, a weak, yet bound, encounter is possible if $R_{\rm peri}$ is large enough. These qualifications are obvious.

For our purposes (that is, matching the disturbances seen in our simulations to those observed at the telescope), we must also be concerned with the duration of pericenter passage Δt. Lines of constant Δt, for which $R_{\rm peri} \propto V_{\rm peri}$, are drawn in Figure 4 as rays whose origin is the origin (not shown) of the $R_{\rm peri} - V_{\rm peri}$ coordinate system. The three lines represent $\Delta t/\tau_{\rm cross} = 2/3$, 1, and 3/2, where $\tau_{\rm cross} = 0.42$ is the internal stellar crossing time within our model galaxy (eq. [24] of Paper I). Larger values of Δt correspond to lines of increasingly steeper slope in the $R_{\rm peri} - V_{\rm peri}$ diagram. To see the importance of pericenter passage duration, consider two cases with equal tidal impulse: one with a small value of $R_{\rm peri}$ (Fig. 5) and one with a large value (Fig. 6). For a fixed tidal impulse, when $R_{\rm peri}$ is very small, $V_{\rm peri}$ must be very large, and, consequently, pericenter passage is extremely fast. In this case, the galaxies may separate to quite a distance before the effects of the tides are visually evident. When they do appear, those tidal

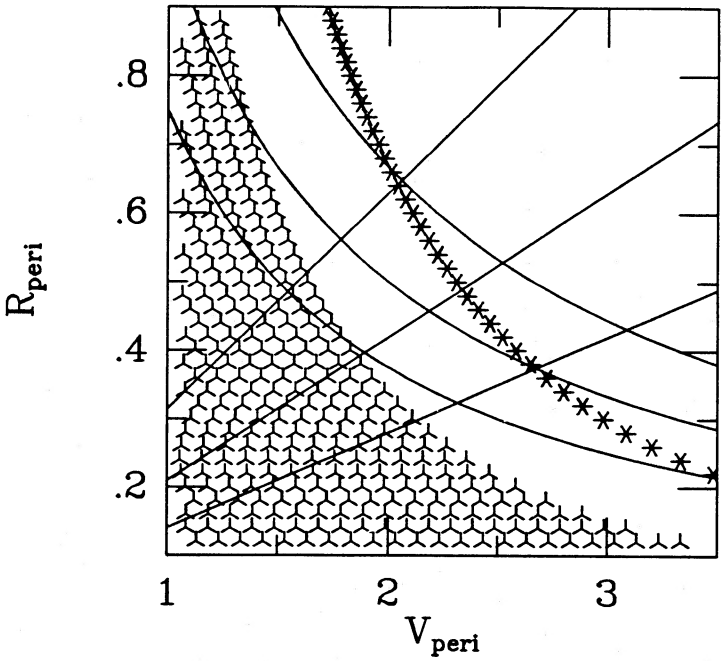

FIG. 4.—$R_{\rm peri} - V_{\rm peri}$ diagram used to describe binary orbital configurations. Lines and curves are discussed in the text.

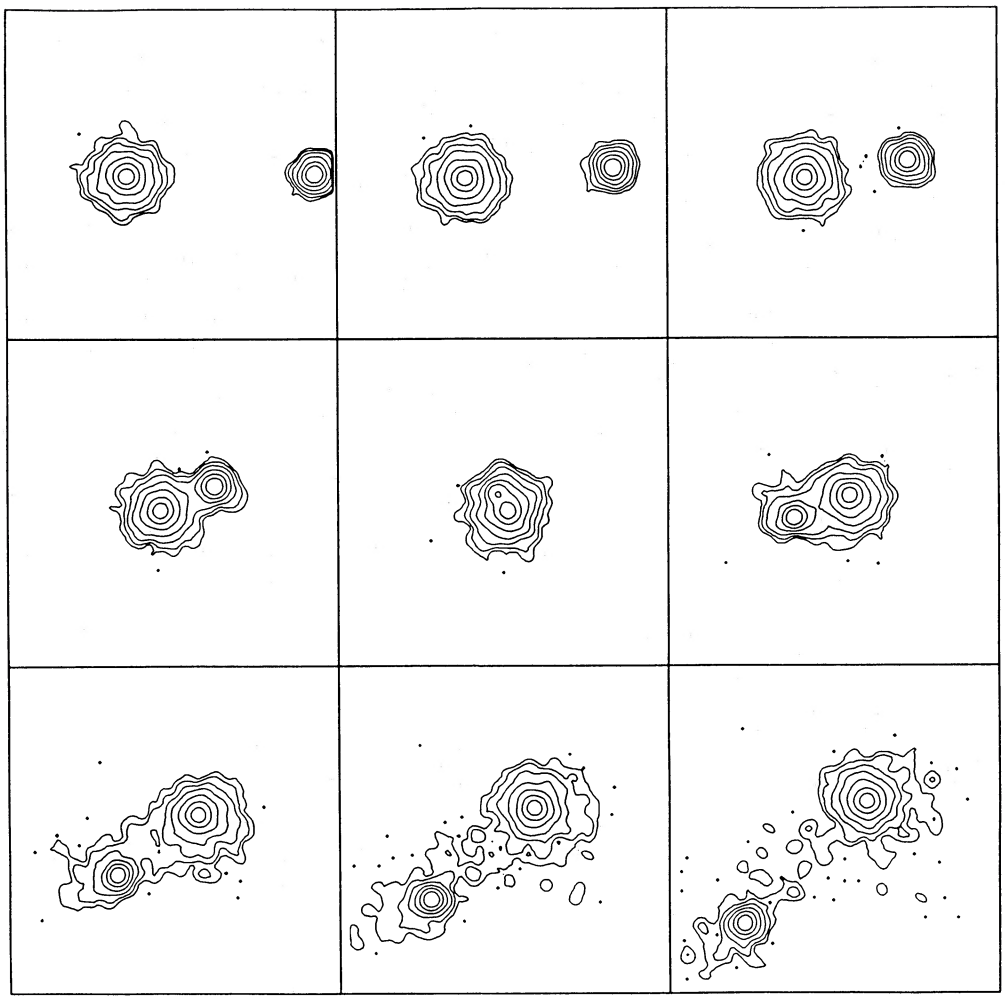

FIG. 5.—Time evolution sequence of an encounter for which $R_{peri} = 0.35$, $V_{peri} = 3.00$, and $M_2/M_1 = 1/3$. Top views of the surface density distribution are spaced at intervals of 0.5 time units, with pericenter passage occurring in the central box of the sequence. Each view is centered on the system center of mass. Contours are calculated as in Fig. 3.

effects can be spectacular. An example of this would be the typical ring galaxy, formed in an $R_{peri} \approx 0$ collision with a second galaxy: the tremendous inward acceleration of the stars in the target galaxy generated by the passage of a massive perturber through its center will become visible as a ring in the target mass distribution only after the companion galaxy has moved to a significant distance from the ring (Lynds and Toomre 1976; Theys and Spiegel 1977; Few and Madore 1986). On the other hand, when R_{peri} is large, pericenter passage is very slow, and significant tidal disturbances will build up before the galaxies have had time to move very far from pericenter.

Figures 5 and 6 demonstrate the two cases of small and large R_{peri} by portraying time evolution sequences of a pair of encounters for which $R_{peri} V_{peri} = 1.05$ and $M_2/M_1 = 1/3$. In each figure, the surface density contour maps represent top views of the encounter at fixed time intervals (0.5 time units, roughly one internal crossing time), with pericenter passage occurring in the central box of each sequence. In Figure 5, $R_{peri} = 0.35$ and $V_{peri} = 3.00$, while $R_{peri} = 0.70$ and $V_{peri} = 1.50$ in Figure 6. Since each binary evolves as a result of energy and angular momentum transfer from the bulk orbital motion into the internal degrees of freedom of each galaxy, the osculating elements of the orbits vary with time. At the time corresponding to the last frame in each sequence: $R_{peri} = 0.33$ and $V_{peri} = 3.00$ in Figure 5, and $R_{peri} = 0.22$ and $V_{peri} = 2.86$ in Figure 6. Although these pairs of numbers are similar, they correspond to an unbound pair in one case and to a tight binary in the other. In the former case, the distortions are most severe when the galaxies are quite separate; in the latter case, the distortions grow as the galaxies spiral closer together, leading to an eventual merger of the pair. Given the choice of one of these two cases as the orbital configuration for a particular pair of galaxies, one could select the correct orbit by measuring the size and shape of the distortions relative to the current binary separation vector. The distortions brought on by a low-R_{peri} collision are not at all like those induced when R_{peri} is large. It is well to keep in mind however that the true separation and the observed separation are two different things, and a steep projection of a slow, distant encounter can look very similar to the pole-on view of the early stages of a close, fast encounter: both display minimal distortions. Usually the additional constraints imposed by detailed velocity measurements will help distinguish between two similar-looking but otherwise extreme orbital configurations; it requires a very special viewing angle not to measure a very

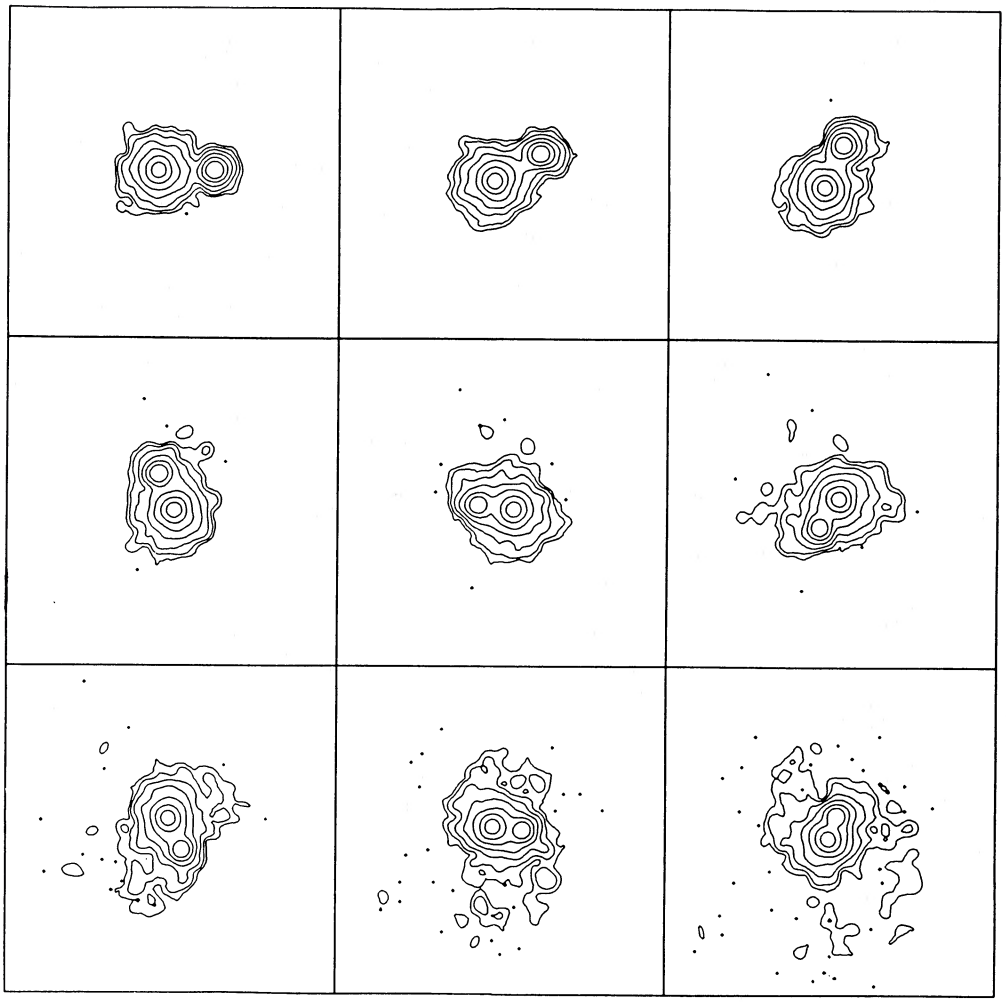

FIG. 6.—Same as Fig. 5, except that the parameters of the initial orbit were: $R_{peri} = 0.70$ and $V_{peri} = 1.50$

high relative speed between the two galaxies in a close, fast passage. Fortunately, a distant, weak encounter cannot look anything like a close, strong encounter, even in projection, if the tidal disturbances in the strong collision have already seriously affected the mass distribution. These significantly perturbed systems are precisely those that we have chosen for study; their solutions occupy a small region of the $R_{peri} - V_{peri}$ diagram and are therefore less ambiguous than the solutions for the weakly disturbed systems.

It is now easy to visualize from Figure 4 that there is a unique limited region in $R_{peri} - V_{peri}$ space which contains all possible matching simulations for a given interacting binary. As described above, encounters that are nearly head-on, with small R_{peri}, tend to have distortions roughly along the line connecting the galaxy centers, while large impact parameter collisions, with larger R_{peri}, portray a phase lag between the distortions and the line of centers. In the latter case, the phase lag will vary with distance from the galaxy center in a manner dependent on the duration of pericenter passage; different depths in the galaxy potential well experience tidal impulses from different directions during a slow encounter, whereas all depths will sense the impulse from the same direction in a very fast collision (the classical impulse approximation). Accordingly, only a narrow range of values are allowed for R_{peri} and any orbit with a value outside that range will give tidal distortions that not only have the wrong orientation and shape, but also those distortions will be either too strong or too weak. The depth within the galaxy to which the tides have disturbed the stars also depends on the collision parameters since fast encounters do not allow enough time for the inner regions to be disturbed, except when R_{peri} is very small. If the inner regions are distorted and the overall distortions are nearly aligned with the companion galaxy, then the pair surely had a small pericenter separation. If the inner regions are distorted and the global distortions are not aligned in any particular manner, then the collision was probably a slow, long-duration, more distant encounter. The smallest radius at which distortions can be detected determines the strength of the tidal impulse: distortions at very small radii indicate a very strong encounter, whereas the lack of distortions even at intermediate radii are indicative of a very weak encounter. Since the magnitude of the tidal impulse is thereby constrained by observation, then so is the speed of the encounter V_{peri}. Encounters that are either faster or slower than that will have a smaller or larger effect, respectively, on the galaxy mass distribution at a given radius. In brief, since the shape of the observed tidal distortions and their orientation relative to the binary separation vector restrict the value of R_{peri}, while the magnitude and radial varia-

tions of the distortions restrict the value of V_{peri}, it is therefore possible to restrict the dynamical solution for a given interacting binary to a single, unique position in Figure 4.

How does all this work in practice? The procedure begins by choosing a value for the binary mass ratio. It is easiest to use the luminosity ratio, and that is what is normally done. The mass ratio computed from equation (13) with the observed central velocity dispersions is also used in some of the simulations. Given the mass ratio, orbits are then systematically studied in $R_{peri} - V_{peri}$ space in a search for encounters that lead to the correct tidal perturbations: correct in size, shape, and orientation relative to the companion galaxy. Time of observation (orbital phase) and orbital inclination are selected by matching the line-of-sight relative velocity and the detailed appearance of the tidal distortions. Clearly, these various steps are not disjoint, but they work together towards finding the one unique spatial + dynamical solution. Internal galaxy parameters (i.e., rotation and flattening) are adjusted as needed to match the properties of the unperturbed inner regions. To play this match game successfully, a large number of binary models must be run and scrutinized from many different viewing angles at many different epochs of their evolution. This would not be possible without the speed and efficiency inherent to MTBA.

To summarize, there is a complicated interplay among the photometric and spectroscopic observations of an interacting binary that restricts the best matching models to a unique, limited domain of model parameter space. Some parameters may easily lead to simulations that are morphologically correct, but which kinematically bare little resemblance to the spectroscopic data. This is precisely the point that deserves the most emphasis. There are very few restictions that can be placed on the solution without the application of kinematic data. A large volume of parameter space will lead to simulations that match only the morphological data, and there may even be one simulation that spells "ALAR TOOMRE" on the sky (Toomre 1974). By working with one more phase space dimension (i.e., the line-of-sight velocity), one can reduce considerably the volume of parameter space containing acceptable dynamical solutions.

Observations of two specific interacting binaries (i.e., Karachentsev 1972, Nos. 99 and 564) are described in Paper III, while Paper IV presents dynamical solutions for each of these two pairs. The differences between the various simulations presented for a given pair identify the probable range of acceptable values for the dynamical parameters as allowed by the observations and, hence, measure the uncertainties in the physical state finally specified for the pair. Subsequent papers in this series will present matching simulations for a number of other interacting pairs of elliptical galaxies.

I wish to thank my thesis adviser J. E. Gunn for his advice and encouragement. For additional help and suggestions, I thank Caltech Professors J. B. Oke, P. Goldreich, and W. L. W. Sargent, Michigan Professors D. O. Richstone and R. P. Kirshner, and DTM astronomer F. Schweizer. I extend special thanks to an anonymous referee for many valuable remarks and recommendations. This research has been supported in part by NSF grant 82-02930 to the University of Michigan, and in part by a Carnegie Fellowship at the Department of Terrestrial Magnetism, Carnegie Institution of Washington.

REFERENCES

Borne, K. D. 1979, *Bull. AAS*, **11**, 673.
———. 1982, Ph.D. thesis, Caltech.
———. 1984, *Ap. J.*, **287**, 503 (Paper I).
———. 1988, *Ap. J.*, **330**, 61 (Paper IV).
Borne, K. D., Balcells, M., and Hoessel, J. G. 1988, *Ap. J.*, submitted (Paper V).
Borne, K. D., and Hoessel, J. G. 1984, *Bull. AAS*, **16**, 881.
———. 1988, *Ap. J.*, **330**, 51 (Paper III).
Borne, K. D., and Richstone, D. O. 1982, *Bull. AAS*, **14**, 972.
———. 1988, preprint.
Burstein, D., and Rubin, V. C. 1985, *Ap. J.*, **297**, 423.
Carlberg, R. G. 1982, *M.N.R.A.S.*, **199**, 1159.
Davies, R. L., Efstathiou, G., Fall, S. M., Illingworth, G., and Schechter, P. L. 1983, *Ap. J.*, **266**, 41.
Faber, S. M., and Jackson, R. E. 1976, *Ap. J.*, **204**, 668.
Farouki, R. T., and Shapiro, S. L. 1982, *Ap. J.*, **259**, 103.
Few, J. M. A., and Madore, B. F. 1986, *M.N.R.A.S.*, **222**, 673.
Gerhard, O. E. 1981, *M.N.R.A.S.*, **197**, 179.
Hoessel, J. G., Borne, K. D., and Schneider, D. P. 1985, *Ap. J.*, **293**, 94.
Illingworth, G. 1981, in *The Structure and Evolution of Normal Galaxies*, ed. S. M. Fall and D. Lynden-Bell (Cambridge: Cambridge University Press), pp. 27–41.
Karachentsev, I. D. 1972, *Comm. Spec. Ap. Obs. USSR*, **7**, 3.
Lynds, R., and Toomre, A. 1976, *Ap. J.*, **209**, 382.
Negroponte, J., and White, S. D. M. 1983, *M.N.R.A.S.*, **205**, 1009.
Schweizer, F. 1982, *Ap. J.*, **252**, 455.
Terlevich, R., Davies, R. L., Faber, S. M., and Burstein, D. 1981, *M.N.R.A.S.*, **196**, 381.
Theys, J. C., and Spiegel, E. A. 1977, *Ap. J.*, **212**, 616.
Toomre, A. 1974, in *IAU Symposium 58, The Formation and Dynamics of Galaxies*, ed. J. R. Shakeshaft (Dordrecht: Reidel), p. 363.
———. 1977, in *The Evolution of Galaxies and Stellar Populations*, ed. B. M. Tinsley and R. B. Larson (New Haven: Yale University Observatory), pp. 401–416.
Villumsen, J. 1982, *M.N.R.A.S.*, **199**, 493.
———. 1983, *M.N.R.A.S.*, **204**, 219.
White, S. D. M. 1978, *M.N.R.A.S.*, **184**, 185.
———. 1979, *M.N.R.A.S.*, **189**, 831.
White, S. D. M., and Sharp, N. A. 1977, *Nature*, **269**, 395.
Wilson, C. P. 1975, *A.J.*, **80**, 175.

KIRK D. BORNE: Space Telescope Science Institute, Homewood Campus, Baltimore, MD 21218